

Correlation between microstructure and magnetotransport in organic semiconductor spin valve structures

Yaohua Liu,¹ Shannon M. Watson,² Taegweon Lee,³ Justin M. Gorham,⁴ Howard
E. Katz,³ Julie A. Borchers,² Howard D. Fairbrother,⁴ and Daniel H. Reich^{1,*}

*¹Dept. of Physics and Astronomy,
The Johns Hopkins University, Baltimore, MD, 21218*

*²NIST Center for Neutron Research,
National Institute of Standards and Technology,
Gaithersburg, Maryland 20899, USA*

*³Dept. of Materials Science and Engineering,
The Johns Hopkins University, Baltimore, MD, 21218*

⁴Dept. of Chemistry, The Johns Hopkins University, Baltimore, MD, 21218

(Dated: February 6, 2020)

Abstract

We have studied magnetotransport in organic-inorganic hybrid multilayer junctions. In these devices, the organic semiconductor (OSC) Alq₃ (tris(8-hydroxyquinoline) aluminum) formed a spacer layer between ferromagnetic (FM) Co and Fe layers. The thickness of the Alq₃ layer was in the range of 50-150 nm. Positive magnetoresistance (MR) was observed at T = 4.2 K in a current perpendicular to plane geometry, and these effects persisted up to room temperature. The devices' microstructure was studied by X-ray reflectometry (XRR), Auger electron spectroscopy (AES) and polarized neutron reflectometry (PNR). The films show well-defined layers with modest average chemical roughness (3-5 nm) at the interface between the Alq₃ and the surrounding FM layers. Reflectometry shows that larger MR effects are associated with smaller FM/Alq₃ interface width (both chemical and magnetic) and a magnetically dead layer at the Alq₃/Fe interface. The PNR data also show that the Co layer, which was deposited on top of the Alq₃, adopts a multi-domain magnetic structure at low field and a perfect anti-parallel state is not obtained. The origins of the observed MR are discussed and attributed to spin coherent transport through a thick layer of Alq₃ (~ 70 nm). However, the subtle correlations between microstructure and magnetotransport indicate the importance of interfacial effects in these systems.

PACS numbers: 72.25.Dc, 72.80.Le, 85.75.-d

I. INTRODUCTION

There is currently a rapidly increasing interest in spin-dependent electronic transport in organic semiconductors. At its heart is the expectation that weak spin-orbit coupling in these light-element-based materials will lead to long spin relaxation times and long spin coherence lengths that may ultimately enable their use in magnetoelectronic devices. In addition, the wide range of organic semiconductors (OSCs) and the ability to tune their properties by suitable chemical modifications holds promise for increased flexibility in controlling spin injection and matching interface properties in multilayered devices such as spin valves. Although it has been generally accepted that there is a conductivity mismatch problem for spin injection from ferromagnetic (FM) contacts into semiconductors,¹ Ruden and Smith² pointed out that, for the case of OSCs, this problem potentially can be solved via a spin-dependent barrier. This barrier layer might be either a Schottky barrier or an insulating interface layer.^{2,3,4} Experimentally, large magnetoresistance (MR) effects were originally reported in FM1/OSC/FM2 trilayers, where the bottom ferromagnetic layer was $\text{La}_{0.67}\text{Sr}_{0.33}\text{MnO}_3$ (LSMO), the OSC was tris(8-hydroxyquinoline) aluminum (Alq_3), and the top FM layer was Co.⁵ Such effects have since been observed for a range of OSCs^{6,7} and in devices where both FM layers are transition metals.^{3,8,9}

However, the nature of the spin transport in these multilayer devices remains unclear, and both spin coherent transport^{5,6,7,8} and spin polarized tunneling^{3,10} have been invoked to explain the observed MR. Furthermore, it is challenging to distinguish among competing theories as reproducibility of sample quality has been an issue in many experimental studies in organic spintronic devices.^{9,11,12} Samples grown by different groups do not consistently show large MR effects,^{8,13} presumably due to subtle structural variances. Particularly problematic has been the question of the degree of interdiffusion of the top FM layer into the much softer OSC layer during sample fabrication.^{5,14} Thus experiments that relate directly the physical and magnetic structure of FM1/OSC/FM2 systems with the existence or non-existence of large MR effects in such structures are essential. In particular, X-ray reflectometry (XRR)^{15,16} and polarized neutron reflectometry (PNR),¹⁷ with their ability to probe the structural and magnetic properties of buried interfaces, are well suited to this task. Here we report XRR and PNR results, in conjunction with SQUID magnetometry, Auger depth profiling, and electrical transport studies to correlate the microstructure and

magnetotransport in OSC spin valve structures.

Our patterned devices used Fe and Co as the top and bottom FM electrodes and Alq₃ with thickness from 50 nm to 150 nm as the spacer layer. Positive magnetoresistance (MR) was observed at T = 4.2 K and these effects persisted up to room temperature. The microstructure was studied by XRR, Auger electron spectroscopy (AES), and PNR on a series of unpatterned films that were co-deposited with the samples used for the transport and magnetization studies. These films showed well-defined layers with modest average chemical roughness (3-5 nm) at the interface between the Alq₃ and the surrounding FM layers. By comparing samples with similar Alq₃ thicknesses, but with different magnetotransport properties, we found direct correlation between the MR amplitude and the microstructure at the FM/Alq₃ interfaces. The magnetic interface is generally smoother than the chemical interface at the Fe-Alq₃ boundary. Larger MR effects are associated with smaller FM/Alq₃ interface widths and with a magnetically dead layer at the Alq₃/Fe interface. Such magnetically dead interfaces may circumvent the resistance mismatch problem² and facilitate effective spin injection.

II. SAMPLE FABRICATION

Co/Alq₃/Fe samples were prepared in thermal evaporation chambers with a base pressure of 2 μ Torr. The films were deposited on Si wafers with 300 nm SiO₂ top layers. Commercially purchased Alq₃ was purified by sublimation before evaporation. The bottom FM film (typically 25 nm Fe) was first deposited at ambient temperature. For transport samples, a shadow mask was used to define the Fe layer into rectangles 6 \times 0.8 mm². Without breaking vacuum, the shadow mask was removed to deposit Alq₃. The Alq₃ thickness was varied from 50 nm to 150 nm. The vacuum chamber was then opened to change shadow masks to permit fabrication of cross junctions for transport measurements. A second FM layer consisting of 5 nm Co and a 40 nm Al capping layer were then deposited in a rectangle 6 \times 0.8 mm² with its long axis perpendicular to the Fe strip. The Fe and Co were deposited at a rate of 0.2 nm/s, the Al was deposited at 0.4 nm/s and the Alq₃ was deposited at 0.1 nm/s. In order to stabilize the OSC films during evaporation and to reduce the potential penetration of Co atoms into the OSC, chilled water was used to keep the substrate holder at 20 °C during Co and Al deposition. The active junction area for the transport samples was 800 \times 800

μm^2 and the unpatterned samples used for reflectivity studies had dimensions $16 \times 16 \text{ mm}^2$. The film thickness was monitored by a quartz crystal oscillator during evaporation and the actual thickness of each layer was determined from the reflectivity experiments.

III. EXPERIMENTAL METHODS

A standard four probe configuration was used for the magnetotransport measurements. The measurements were carried out in a continuous flow cryostat in the temperature range from 4 K to 290 K. An in-plane magnetic field in range of $\pm 200 \text{ mT}$ was applied parallel to the top Co electrode to control the relative magnetization direction of the top and bottom FM layers. Magnetic hysteresis loops of the films were obtained using a SQUID magnetometer at a series of temperatures. The films' structure was studied by X-ray reflectometry, using a 4-circle diffractometer. The X-ray source uses a ceramic filament tube with a Cu-target. $\Omega - 2\theta$ scans were performed, where Ω is the angle between the incident beam and the sample surface, and 2θ is the scattering angle. A pair of Soller slits with divergence 0.04° were used in the beam path to limit the axial divergence of the X-ray beam. A curved graphite monochromator was used to filter the Cu K_β line, leaving Cu K_α radiation with wavelength $\lambda = 1.5417 \text{ \AA}$. In a typical specular reflectivity scan, 2θ varied from 0° to 5° , with resolution better than 0.01° . Background data were obtained using a 0.1° offset in Ω . Elemental depth profiling was carried out using a Scanning Auger Microprobe. Auger electrons were collected in three energy windows for a series of sputtering cycles. In each cycle, the sample was sputtered for 2 minutes with Ar ions and then Auger electrons were collected as a function of kinetic energy with energy step 1 eV over the ranges 745 eV to 790 eV, 245 eV to 295 eV, and 560 eV to 610 eV. These ranges isolate the Co LVV, C KLL, and Fe LMM characteristic peaks, respectively.

To identify the devices' spin structures, we employed PNR techniques¹⁸ to determine the depth-dependent vector magnetization of individual FM layers on sub-nanometer length scales, using the NG-1 polarized neutron reflectometer at the NIST Center for Neutron Research. For the PNR experiments, neutrons were polarized parallel to the applied field in the sample plane. A vertically-focusing pyrolytic graphite monochromator was used to select neutrons with wavelength of 4.75 \AA and a wavelength divergence of 0.05 \AA . The neutron beam had an angular divergence $\delta\theta = 0.018^\circ$. By employing two spin flippers,

all four spin scattering cross sections were measured, including two non-spin flip (NSF) reflectivities, $R^{(++)}$ and $R^{(--)}$, and two spin flip (SF) reflectivities, $R^{(+-)}$ and $R^{(-+)}$. For the NSF reflectivities, the neutron retains its original polarization after scattering from the sample, and for the SF reflectivities the neutron changes spin states. The NSF reflectivities provide information concerning the chemical composition of the film and are sensitive to the component of the in-plane magnetization aligned along the field axis. The SF reflectivities are sensitive only to that component of the in-plane magnetization perpendicular to the field direction. Specular reflectivity scans were made over the range of $0^\circ \leq 2\theta \leq 5.2^\circ$. For non-specular reflectivity scans (used for background subtraction), $\Omega = 0.5 \times 2\theta - 0.3^\circ$ and 2θ covered the same range as used in the specular scans. Rocking curves were taken by rotating the sample plane from $\Omega = -1.4^\circ$ to 2.8° while fixing the detector at $2\theta = 1.4^\circ$. The PNR measurements were taken at both $T = 40$ K and room temperature. At each temperature, PNR was measured at two fields, a high field at which the average in-plane magnetization of the Co and Fe were parallel and a low field at which they were antiparallel. These fields were chosen based upon characteristics of magnetic hysteresis loops measured with SQUID magnetometry. Both the X-ray and neutron specular reflectivity data were corrected for instrumental background, efficiencies of the polarizing elements (neutrons only, typically $> 98\%$), and the footprint of the beam. The ReFlpak software suite, which uses a least squares optimization, was used for elements of the XRR and PNR data reduction and analysis.¹⁹

IV. RESULTS AND ANALYSIS

A. Magnetotransport measurements

The chemical structure of Alq_3 is shown in Fig. 1a. Figure 1b shows current-voltage (I-V) curves for a junction with a 64 nm thick Alq_3 layer. These are distinctly nonlinear at low temperatures. As the temperature increases, the I-V curves become more linear, and at the same time both the junction resistance and the MR decrease. The I-V curves show very weak asymmetry for positive bias and negative bias. The maximum MR observed for this sample was 7% at $T = 80$ K and 1% at $T = 290$ K, as shown in Fig. 1c and Fig. 1d, respectively. Both the nonlinear I-V curve and the temperature dependence of the junction resistance

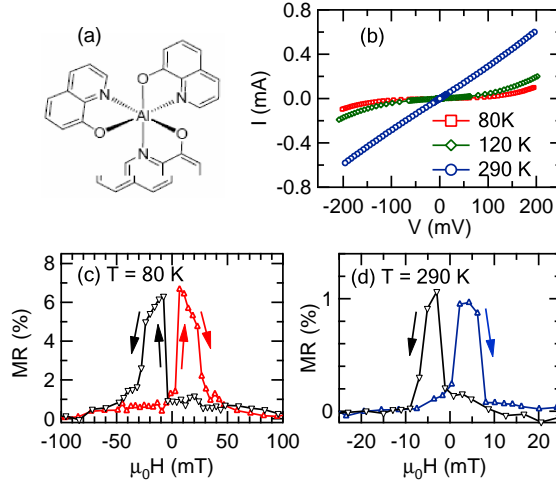


FIG. 1: (a) Chemical structure of Alq₃. (b) I-V curves of a junction with 64 nm Alq₃ spacer layer, taken at $T = 80$ K, 120 K and 290 K. The I-V curves show increased nonlinearity and increasing junction resistance as the temperature decreases. (c) and (d) show the magnetoresistance data of this device taken at $T = 80$ K and 290 K, respectively. The data were taken with four probe configuration, and a DC current $I = 1 \mu\text{A}$. The high field resistances were 22.2 k Ω at 80 K and 355 Ω at 290 K.

exclude the possibility of a metallic short between the two FM layers in this sample.⁶

To illustrate the relationship between the magnetic switching of the Co and Fe layers and the observed MR of these structures, a magnetic hysteresis loop is shown overlaid with magnetotransport data in Fig. 2a for a junction with an 85 nm Alq₃ layer. Both data sets were taken at $T = 80$ K with the magnetic field parallel to the Co strip. This sample showed a maximum 3% MR at $T = 80$ K. The hysteresis loop shows a two-step switching of the layers' magnetization. When the field was swept from -200 mT to 200 mT, the net magnetization abruptly changed sign at $\mu_0 H \approx 5$ mT. This large change arises from the magnetization reversal of the Fe layer, which is approximately three times as thick as the Co layer. As the field is increased above 5 mT, the magnetization gradually approaches saturation. Above $\mu_0 H \approx 80$ mT, the magnetization is essentially saturated. The sample shows a rise in MR that correlates with the nominal Fe magnetization reversal at $\mu_0 H \approx 5$ mT, followed by decreasing MR with increasing field. When $\mu_0 H \geq 80$ mT, no apparent hysteresis in either the magnetization or the MR is observed. Figure 2b shows similar data taken at $T = 290$ K. Here, the magnetization reversal happened at a lower field, $\mu_0 H \approx$

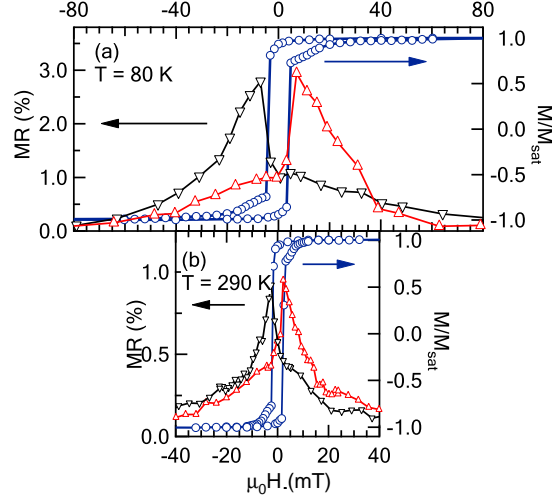


FIG. 2: (a) Magnetoresistance data (triangles) and the hysteresis loop (blue circles) for a sample with Alq_3 thickness = 85 nm. Both data sets were taken at $T = 80$ K with the magnetic field parallel to the Co strip. The magnetoresistance shows a jump at the same field where the magnetization along the field changes its sign, i.e. at $\mu_0 H \approx \pm 5$ mT. (b) Similar data taken at $T = 290$ K. The sudden changes of the magnetoresistance and magnetization occur at lower fields, $\mu_0 H \approx \pm 2.5$ mT, than at $T = 80$ K. The measurement current was $I = 10 \mu\text{A}$ and the high field resistance was 640Ω at 80 K and 25Ω at 290 K.

± 2.5 mT. This is characteristic behavior of a spin valve device where the high and low resistance states come from the configurations with antiparallel and parallel alignment of the magnetization of the FM layers, respectively. The shift to lower field is presumably due to a decrease in the barrier to switching with increasing temperature.

Magnetotransport properties were measured for a series of junctions with Alq_3 thicknesses from 50 nm to 150 nm. For each set of junctions with the same Alq_3 thickness, magnetotransport measurements were performed on 6 - 12 samples. The results are summarized as maximum MR observed in a sample as a function of the sample's resistance for 3 sets of junctions, as shown in Fig. 3. These junctions are labeled by the thickness of the Alq_3 layer. Both room temperature and $T = 80$ K results are shown. The set of junctions with 124 nm Alq_3 generally have resistances larger than 1 G Ω at $T = 80$ K, which limits our ability to make accurate transport measurements. We found significant variability in both resistance and MR, consistent with what has been observed in other FM/OSC/FM devices up to now.^{9,11,12} Although we confirmed the tendency that the MR increased with decreasing

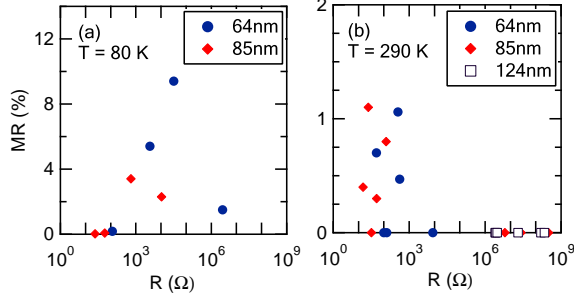


FIG. 3: Maximum MR measured in 3 sets of junctions with different Alq₃ thickness as a function of the junction resistance, data taken at (a) T = 80 K and (b) 290 K, respectively. The maximum MR observed in a set of junctions decreases as the Alq₃ thickness increases. However, there is large variability in both junction resistances and MRs from the same batch.

thickness of the Alq₃ layers, the large variability makes it difficult to obtain the effective spin diffusion length accurately.

B. X-ray reflectivity

X-ray reflectivity was used to study the structure of the spin valve films. An example of data obtained in such measurements is shown in Fig. 4a. The data are shown vs the momentum transfer perpendicular to the film plane $Q_z = 4\pi \sin \theta / \lambda$. The data shown in Fig. 4a are dominated by oscillations with period $\Delta Q \approx 0.004 \text{ \AA}^{-1}$. This corresponds to the total thickness of the Co/Alq₃/Fe trilayer, which is about 160 nm. However, additional modulations of the scattering are also present, which enable full determination of the structural depth profile.

The reflectivity data were fit using the ReFlpak software system,¹⁹ which employs Parratt's algorithm²⁰ to model interface roughness as a sequence of very thin slices whose scattering length density (SLD) and absorption vary smoothly so as to interpolate between adjacent layers in the spin-valve stack. The SLD profile determined in this manner for this sample is shown in Fig. 4b, and the best-fit curve for the reflectivity data is overlaid on the data in Fig. 4a. The principal results determined from these fits are that there are well-defined regions of the film corresponding to the Co, Alq₃, and Fe layers, respectively, and that the interfacial roughnesses are small, typically 3-5 nm, indicating that there is only limited

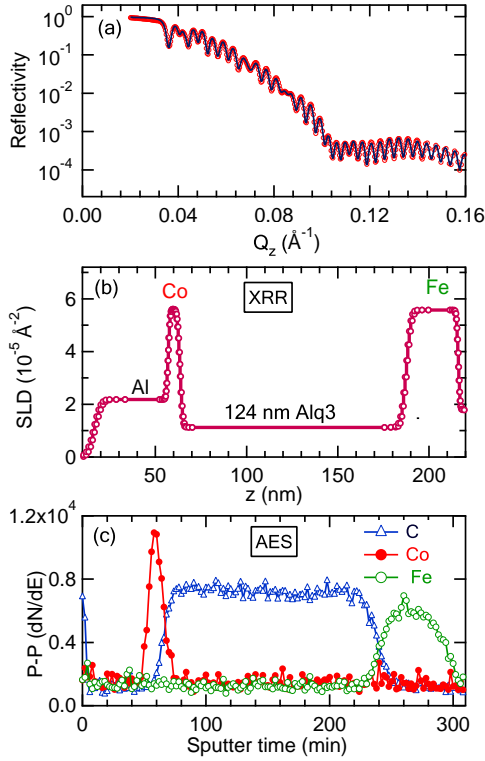


FIG. 4: (a) Specular XRR data (dots) together with the fit (solid line) for a Al/Co/Alq₃/Fe multilayer. (b) The SLD profile acquired from the fit, which shows well defined layer structures. This result is confirmed by the elemental depth profile acquired by AES (c) on a sample from the same batch. In these data, the carbon signal indicates the presence of Alq₃.

mixing between the OSC and FM layers. These results also yield accurate measurements of the individual layer thicknesses. In this case, they are $t_{Co} = 6.44 \pm 0.05$ nm, $t_{Alq_3} = 124.05 \pm 0.05$ nm, and $t_{Fe} = 28.51 \pm 0.05$ nm.

To confirm the accuracy of the XRR results, the elemental composition of a second film co-deposited with that shown in Figs. 4a and 4b was measured by AES depth profiling. In AES, the peak to peak height of the count rate differentiated with respect to the energy $dN/d\epsilon$ is proportional to the concentration for each probed element. These results are shown in Fig. 4c, where the differential peak to peak heights are plotted as a function of sputtering time. The average sputtering rate was approximately 0.7 nm/s. The structure of the layers can also be inferred from these data, and are seen to be consistent with the XRR data.

Figure 5 shows XRR data for three films with comparable Alq₃ thicknesses: 85 nm, 81 nm and 94 nm, respectively. The insets in Figure 5 show magnetotransport data on

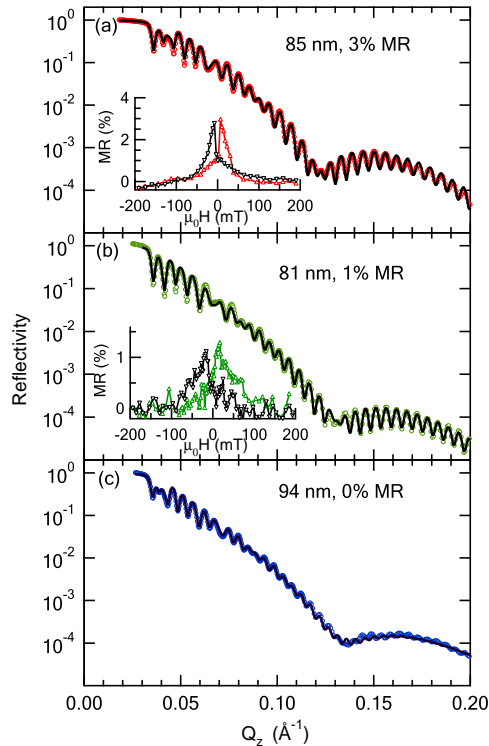


FIG. 5: XRR data and fits for three films with comparable Alq_3 thicknesses, (a) 85 nm , (b) 81 nm and (c) 94 nm, respectively. The insets in (a) and (b) show the magnetotransport data on junctions co-deposited with these films taken at 80 K (a) and 10 K (b). The maximum MR observed was 3%, 1% and 0%, respectively.

junctions co-deposited with these films, which show maximum MR of 3% (Figure 5a), 1% (Figure 5b) and 0% (Figure 5c). Hereafter, we will label these samples as the 3%, 1% and 0% MR samples. (The 3% MR sample is the same one as that shown in Fig. 2.) The depth dependence of the SLD for the three samples as determined from the fits to the reflectivities is plotted in Fig. 6(a)-(c). The best-fit Co SLDs are about 10% lower than the bulk values and varied from sample to sample in a range of 10%. For the 3% MR sample, the best-fit Fe SLD is bulk-like, but for the 1% and 0% MR samples, it is $\sim 7\%$ lower than the bulk value, possibly indicative of voids or strain which reduce the average density. The measured SLD of the Alq_3 layers $QC_{\text{Alq}_3} = 1.16 \times 10^{-5} \text{ \AA}^{-2}$ and varies by less than 2% from sample to sample. Details of the SLD depth profiles at the interfaces between the FM layers and the OSC are shown in Fig. 6(d)-(e). In order to compare the interfacial variation of SLDs among different samples, we introduced the parameter δz , which is the depth z with an

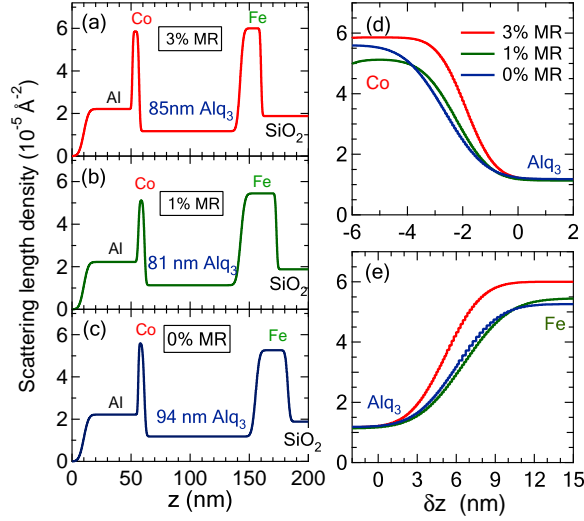


FIG. 6: (a)-(c) SLD from fitting the XRR data for three samples with similar Alq₃ thicknesses but different MRs. (d) and (e) Details of the structural roughnesses at the interfaces between the FM metals and Alq₃. Offsets in z were applied to align the curves at the FM/Alq₃ interfaces. δz is defined as the distance with respect to a point near the Alq₃ side, where $QC_{nor}(z) = 0.01$. $QC_{nor}(z) = (QC(z) - QC_{Alq_3}) / (QC_{FM} - QC_{Alq_3})$, where QC_{Alq_3} and QC_{FM} are the fit values of the SLDs for the Alq₃ layer and the appropriate FM layer.

offset (see the caption for definition) in order to align the data at the FM/Alq₃ interfaces. A clear correlation between the maximum observed MR and the widths of the FM/Alq₃ interfaces was observed, with sharper interface width corresponding to larger MR. The fits are more sensitive to the structure at the Co/Alq₃ interface than to that at the Alq₃/Fe interface. The widths (10% - 90%) are 2.1 nm, 2.5 nm, and 2.9 nm at the Co/Alq₃ interface and 5.7 nm, 7.2 nm, and 6.4 nm at the Alq₃/Fe interface for the 3% MR, 1% MR and 0% MR samples, respectively.

C. Polarized neutron reflectivity

Studies on metallic SV structures have shown that the chemical structure alone is not sufficient to determine magnetotransport properties.¹⁷ We therefore employed PNR to explore the depth-dependent magnetic structure in these samples. PNR was measured for each sample at $T = 40$ K and 290 K, and at two fields for each temperature. The measurement fields were chosen based on magnetic hysteresis loops taken at each temperature, such as

those shown in Fig. 2 at 80 K and 290 K for the 3% MR sample. The high field PNR data for all samples were taken at $\mu_0 H = 200$ mT, where the magnetization of both the Co and Fe layers were saturated parallel to H. The low field state was prepared by sweeping the field from -200 mT to a small positive field just above the abrupt increase in $M(H)$ where the Fe magnetization appears to reverse direction (e.g., Fig. 2). For the 3% MR sample at 40 K, the Fe layer switching occurred at $\mu_0 H = 8$ mT, and the PNR measurements were made at 10 mT.

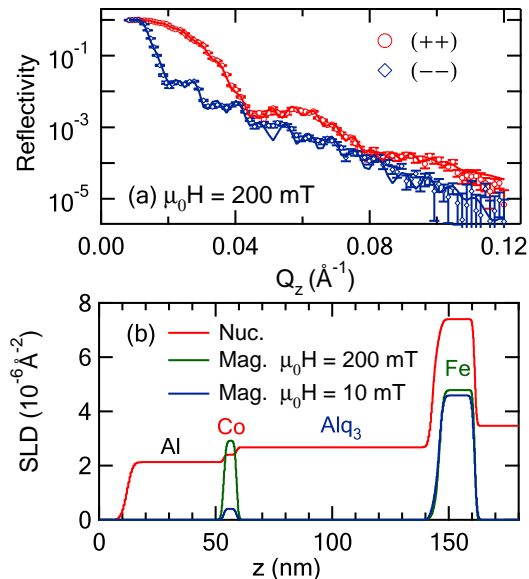


FIG. 7: (a) High field ($\mu_0 H = 200$ mT) specular reflectivity data (circles) with fits (solid lines) of the two NSF cross sections, $R^{(++)}$ and $R^{(--)}$, for the 3% MR sample. The data were taken at $T = 40$ K. (b) The nuclear and magnetic SLDs obtained from the fits.

The PNR data obtained in a high saturating field for all three samples are typified by the data shown for the 3% sample in Fig. 7a. All of our specular SF reflectivity scans had negligible scattering (data not shown), which indicates no net moment aligned perpendicular to the applied field. In order to obtain a reasonable fit to the high-frequency oscillations in the $R^{(--)}$ cross section, it was necessary to divide the Fe layer into two sections with independently-varying values of the magnetic SLD. The nuclear and magnetic SLD profiles determined from the fits are shown in Fig. 7b. The magnetic SLD does not track the nuclear SLD as the magnetized region of the Fe layer does not fully extend to the nuclear Alq_3/Fe interface. In order to see the difference more clearly, we plot the normalized nuclear and

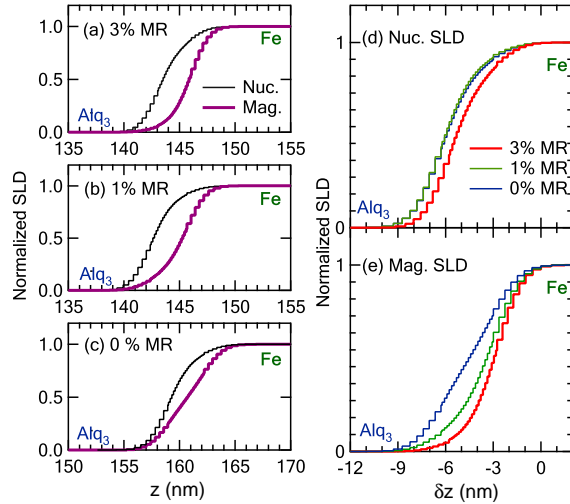


FIG. 8: Normalized nuclear and magnetic SLDs at the Alq₃/Fe interface for (a) 3% MR, (b) 1% MR and (c) 0% MR samples, respectively. These values are obtained for data taken at $T = 40$ K and $\mu_0 H = 200$ mT. Different depth dependences of the nuclear and magnetic SLDs were observed at the Alq₃/Fe interface. The normalized nuclear SLD QN_{nor} (d) and the normalized magnetic SLD QM_{nor} (e) for all three samples. δz is defined as the distance with respect to a point near the Fe side, where $QM_{nor}(z) = 0.99$. The sample showing the largest MR has the sharpest magnetic interface, while the difference in the nuclear SLDs is much smaller.

magnetic SLDs for each of the three samples in Fig. 8a-c, using a definition similar to that used for the XRR data. For direct comparison, the normalized nuclear SLDs at the Alq₃/Fe interface for all the three samples are plotted in Fig. 8d along with the normalized magnetic SLDs in Fig. 8e. The trends in the nuclear SLDs are similar to those identified from the X-ray reflectivity data (Fig. 6) with the 3% sample showing the sharpest Alq₃/Fe interface. Since the magnetic hysteresis data (Fig. 2) indicate that the magnetization is saturated in this field of 200 mT, we conclude that the difference between the nuclear and magnetic for each sample (Fig. 8a-c) corresponds to a region of the Fe layer near the Alq₃/Fe interface in which the magnetization is suppressed. The observation of a magnetically dead layer is not a total surprise and has been reported for several magnetic multilayer structures.^{21,22,23} It is notable that the sample showing the largest MR has the largest magnetic dead region near the Alq₃/Fe interface (Fig. 8e).

The low-field reflectivity data at 40 K (Fig. 9) show features, especially in the $R^{(-)}$

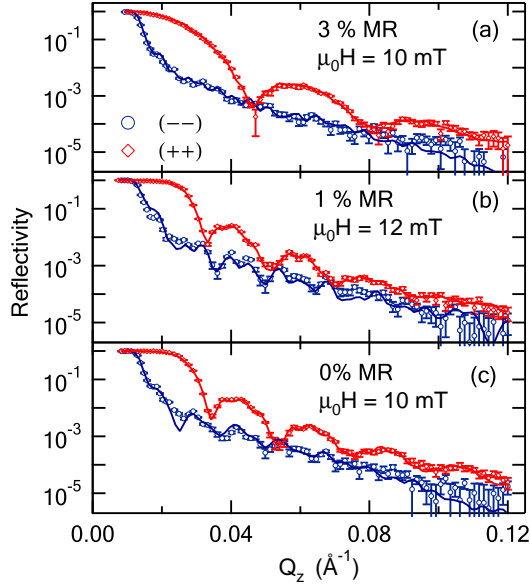


FIG. 9: Low field NSF PNR data and best fits for the (a) 3%, (b) 1% and (c) 0% MR sample, respectively. Data were taken at $T = 40$ K.

cross section, that differ substantially from those in the high-field data (e.g., Fig. 7a). Fits to the data for all three samples (Fig. 9a-c) reveal that the magnetically dead layer near the Alq_3/Fe interface persists (e.g., Fig. 7b), and that the Co layers' moments are aligned antiparallel to the Fe layers' moments, as expected from the magnetization curves. However, while the fitted moment of the Co layers for the 0% and 1% MR samples nearly matches the Co saturation moment (Table I), the damped oscillations in the $R^{(-)}$ data for the 3% MR sample (Fig. 9a) are best fit with a model in which the Co magnetization, averaged across the sample plane, is greatly reduced from its bulk value. This small, net Co moment is aligned antiparallel to the Fe moment (Table I).

	3% MR	1% MR	0% MR
High Field	2.9	3.4	2.8
Low Field	-0.4	-2.0	-2.8

TABLE I: Summary of high field and low field in-plane magnetic SLDs of the Co layer at $T = 40$ K for 3 different samples. The data are in units of 10^{-6} \AA^{-2} . The minus sign of the SLDs at low field indicates that the magnetization of the Co layer is antiparallel to the external field.

The reduction of the Co magnetization for the 3% sample is accompanied by magnetic

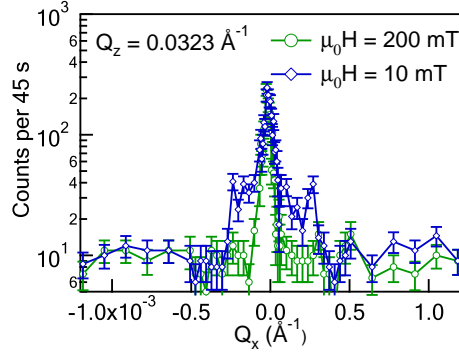


FIG. 10: Spin flip rocking curves of the 3% MR sample taken at $\mu_0H = 200$ mT and 10 mT, respectively. The data were taken at $T = 40$ K and $Q_z = 0.0323$ \AA^{-1} . The enhanced scattering at low field is consistent with the observation of the much smaller Co magnetization along the field direction at low field (Table I). These observations strongly suggest magnetic multi-domain formation at low field.

diffuse scattering in the SF rocking curves, as shown in Fig. 10. The diffuse scattering disappears upon application of a saturating magnetic field of 200 mT, indicating that it likely originates from in-plane magnetic domains.^{24,25} While some diffuse scattering was observed in low fields for the 1% and 0% MR samples, this scattering is most pronounced for the 3% sample. Contrary to the expectation for an ideal spin valve, perfect antiparallel alignment of the Co and Fe moments is thus not achieved in the sample that exhibits the maximum MR. Instead, our PNR results suggest that the Co layer break up into multiple magnetic domains within the sample plane at low field.^{24,25}

The $T = 290$ K PNR data in high and low fields appear superficially similar to the $T = 40$ K data. Figure 11 shows typical data for the 3% MR sample. However, in comparison to the $T = 40$ K data (Fig. 7a), the splitting between the $R^{(++)}$ and $R^{(--)}$ specular reflectivities is smaller at $T = 290$ K. The best-fit values for the magnetic SLD (Table II) show that this originates from a decrease of the in-plane magnetization of the Fe layer. The reduction of the saturation magnetization of the Fe layer from $T = 40$ K to $T = 290$ K is actually much larger than that expected for a thick, bulk Fe film. The magnetic SLD of the Co layer at low field is very small for all three samples and, in general, the fits at low field are much less sensitive to the orientation of the Co magnetic moment relative to the Fe layer. The best fits indicate that the Co layers are aligned parallel to the Fe layers in all three samples at

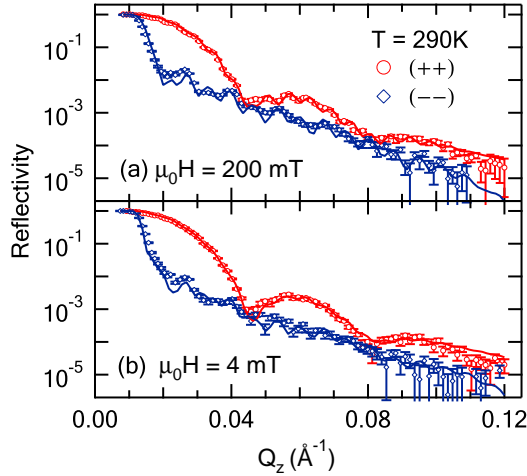


FIG. 11: Specular reflectivity data (circles) of two NSF cross sections taken at $T = 290$ K for 3% MR sample with fits (solid lines). (a) High field $\mu_0H = 200$ mT and (b) low field $\mu_0H = 4$ mT.

low fields. These PNR results are consistent with the observed reduction of the MR at 290 K relative to low temperature.

	Co		Fe	
	High field	Low field	High field	Low field
T = 40 K	2.9	-0.4	4.8	4.6
T = 290 K	2.9	0.8	4.6	4.4

TABLE II: The in-plane magnetic SLDs of the Co and the Fe layers for the 3% MR sample at different experimental conditions. The data are in units of 10^{-6} \AA^{-2} .

V. DISCUSSION

The thickness of the AlQ_3 layer in our samples ranges from 50 nm to 150 nm, which is far above the range where tunneling would be expected to contribute to the magnetotransport. The resistance of the junctions increases quickly as temperature decreases, which argues against the existence of metallic pinholes. Our XRR and AES results suggest that there is no large-scale intermixing between the FMs and the AlQ_3 . It is possible that cobalt atoms that penetrate into the AlQ_3 could behave as dopants due to charge transfer from Co to AlQ_3 .²⁶ However it is very unlikely that the MR behavior is caused by the tunneling of

chains of cobalt nanoclusters for our samples, as suggested by Vinzelberg *et al.*¹⁴ The XRR data show that the concentration of cobalt decays by a factor of 9 over a distance of 2.1 nm at the Co/Alq₃ interface for the sample showing large MR. Therefore assuming an exponential decay of the cobalt concentration, there is approximately 1 cobalt atom for 10¹⁸ atoms inside the Alq₃ matrix at a distance of 40 nm below the cobalt layer. The chance of finding a cobalt cluster of a few nm size is thus very small, and formation of a conductive path of cobalt chains over distance more than 60 nm is highly unlikely. The XRR results show that large MR is also associated with small chemical roughness at the Co/Alq₃ interface. This observation also suggests that the MR is not caused by cobalt chains, because greater roughness would result in a higher probability of forming such chains.

The observed MR is also not caused by anisotropic magnetoresistance (AMR) of the FM leads. We used a four probe configuration, and hence the contribution of the lead resistance is minimized. Furthermore, the resistance of the junction is much larger than that of the leads. The measured amplitude of the AMR of the Fe lead is much smaller than the MR of the junction. Changing the external field direction from parallel to the Co strip to parallel to the Fe strip does not significantly change the shape of the MR curve for the junction, but it causes the AMR curves of the Fe leads to change sign. (The cobalt layer is in parallel with a much thicker nonmagnetic Al layer and hence its AMR is not measurable.)

The I-V curves of our junctions show very weak asymmetry for positive bias and negative bias, as shown in Fig. 1b. It is expected that there would be different charge injection barriers from Fe and Co into Alq₃, based on the work function of pristine metals fabricated and measured in ultrahigh vacuum conditions.¹³ However, the work function of both Fe and Co in contact with OSCs decreases and becomes comparable when fabricated in a vacuum similar to what we used here.²⁷ Therefore similar charge injection barriers at the Co/Alq₃ and Alq₃/Fe interfaces would be expected.

Our XRR/PNR study shows that the observation of large MR is directly related to the sharpness of the chemical interface between the FM layers and the Alq₃ layer, and also to the sharpness of the magnetic interface between the Fe and the Alq₃. In metallic spin valve systems, the same tendency has been observed and attributed to enhanced spin flip scattering due to rough interfaces.¹⁶ Additional interesting results come from the observation of the sharper magnetic interface as compared to the chemical interface at the Alq₃/Fe boundary. Larger MR is correlated to the presence of a magnetically dead region near the Alq₃/Fe

interface which acts as a barrier between the bulk Alq_3 layer and the magnetic Fe layer which acts as a polarized electron reservoir. This magnetically dead interface could behave as a spin injection barrier which helps to circumvent the resistance mismatch issue at the FM/OSC interface.^{2,3,4} At the same time, we observed that as the temperature increases, the in-plane magnetization of Fe in saturation field decreases much more than expected, this may contribute partially to the reduction of observed MR as temperature increases.

The fits to the PNR are less sensitive to the Co magnetic SLD because this layer is much thinner than the Fe layer. However we do find that there is a large reduction of the magnetic SLD of the Co layer at low field as well as strong magnetic diffuse scattering for the sample showing the largest MR. These observations suggest that thin Co films on top of Alq_3 are likely to form multi-domain magnetic structures at low fields and a poorly defined anti-parallel state. This most likely explains the gradual change in MR with increasing field and the lack of a well-defined plateau in the MR in the high resistance state.

VI. CONCLUSION

Our work demonstrates that it is possible to use high T_c FM transition metals to inject spin polarized current into OSCs at room temperature. However, samples fabricated with similar conditions do not show consistent magnetotransport properties. We find that this originates from subtle differences in the microstructure of the samples, especially at the FM/ Alq_3 interfaces. Larger MR is associated with smaller structural roughness at the Co/ Alq_3 and Alq_3 /Fe interfaces, and with a magnetically dead region near the Fe/ Alq_3 interface. The fact that significant MR can be observed in such samples even when an ideal antiparallel state is not formed implies an important role of the interfaces in controlling spin injection from FM metals to OSCs. In addition, the magnetically dead layer we have observed may circumvent the resistivity mismatch problem. Further studies of interfacial effects are needed for these organic systems.

Acknowledgments

This work was supported by NSF Grant No. DMR-0520491. We acknowledge the support of the National Institute of Standards and Technology, U.S. Department of Commerce, in

providing the neutron research facilities used in this work. The AES measurement was carried out in the surface analysis laboratory at Johns Hopkins University.

-
- * Corresponding author, reich@jhu.edu
- ¹ G. Schmidt, D. Ferrand, L. W. Molenkamp, A. T. Filip, and B. J. van Wees, *Phys. Rev. B* **62**, R4790 (2000).
 - ² P. P. Ruden and D. L. Smith, *J. Appl. Phys.* **95**, 4898 (2004).
 - ³ T. S. Santos, J. S. Lee, P. Migdal, I. C. Lekshmi, B. Satpati, and J. S. Moodera, *Phys. Rev. Lett.* **98**, 016601 (2007).
 - ⁴ V. Dediu, L. E. Hueso, I. Bergenti, A. Riminucci, F. Borgatti, P. Graziosi, C. Newby, F. Casoli, M. P. D. Jong, C. Taliani, et al., *Phys. Rev. B* **78**, 115203 (2008).
 - ⁵ Z. H. Xiong, D. Wu, Z. V. Vardeny, and J. Shi, *Nature (London)* **427**, 821 (2004).
 - ⁶ F. J. Wang, C. G. Yang, Z. V. Vardeny, and X. G. Li, *Phys. Rev. B* **75**, 245324 (2007).
 - ⁷ S. Majumdera, R. Laiho, P. Laukkanen, I. J. Väryste, H. S. Majumdar, and R. Österbacka, *Appl. Phys. Lett.* **89**, 122114 (2006).
 - ⁸ F. J. Wang, Z. H. Xiong, D. Wu, J. Shi, and Z. V. Vardeny, *Synthetic Metals* **155**, 172 (2005).
 - ⁹ S. Pramanik, S. Bandyopadhyay, K. Garre, and M. Cahay, *Phys. Rev. B* **74**, 235329 (2006).
 - ¹⁰ W. Xu, G. J. Szulczewski, P. LeClair, I. Navarrete, R. Schad, G. Miao, H. Guo, and A. Gupta, *Appl. Phys. Lett.* **90**, 072506 (2007).
 - ¹¹ J. R. Petta, S. K. Slater, and D. C. Ralph, *Phys. Rev. Lett.* **93**, 136601 (2004).
 - ¹² T. Ikegami, I. Kawayama, M. Tonouchi, S. Nakao, Y. Yamashita, and H. Tada, *Appl. Phys. Lett.* **92**, 153304 (2008).
 - ¹³ J. S. Jiang, J. E. Pearson, and S. D. Bader, *Phys. Rev. B* **77**, 035303 (2008).
 - ¹⁴ H. Vinzelberg, J. Schumann, D. Elefant, R. B. Gangineni, J. Thomas, and B. Büchner, *J. Appl. Phys.* **103**, 093720 (2008).
 - ¹⁵ E. E. Fullerton, D. M. Kelly, J. Guimpel, I. K. Schuller, and Y. Bruynseraede, *Phys. Rev. Lett.* **68**, 859 (1992).
 - ¹⁶ R. Schad, P. Beliën, G. Verbanck, C. D. Potter, H. Fischer, S. Lefebvre, M. Bessiere, V. V. Moshchalkov, and Y. Bruynseraede, *Phys. Rev. B* **57**, 13692 (1998).
 - ¹⁷ M. R. Fitzsimmons, S. D. Bader, J. A. Borchers, G. P. Felcher, J. K. Furdyna, A. Hoffman,

- J. B. Kortright, I. K. Schuller, T. C. Schulthess, S. K. Sinha, et al., *J. Mag. Magn. Mater.* **271**, 103 (2004).
- ¹⁸ C. F. Majkrzak, *Physica B* **173**, 75 (1991).
- ¹⁹ P. A. Kienzle, K. V. O'Donovan, J. F. Ankner, N. F. Berk, and C. F. Majkrzak, <http://www.ncnr.nist.gov/reflpak>, 2000-2006.
- ²⁰ J. F. Ankner and C. F. Majkrzak, in *Neutron Optical Devices and Applications*, edited by C. F. Majkrzak and J. L. Wood (SPIE, 1992), vol. 1738, pp. 260–269.
- ²¹ J. W. Cable, M. R. Khan, G. P. Felcher, and I. K. Schuller, *Phys. Rev. B* **34**, 1643 (1986).
- ²² M. J. Pechan, J. F. Ankner, C. F. Majkrzak, D. M. Kelly, and I. K. Schuller, *J. Appl. Phys.* **75**, 6178 (1994).
- ²³ A. Hoffmann, S. G. E. te Velthuis, Z. Sefrioui, J. Santamaria, M. R. Fitzsimmons, S. Park, and M. Varela, *Phys. Rev. B* **72**, 140407(R) (2005).
- ²⁴ J. A. Borchers, P. M. Gehring, R. W. Erwin, J. F. Ankner, C. F. Majkrzak, T. L. Hylton, K. R. Coffey, M. A. Parker, and J. K. Howard, *Phys. Rev. B* **54**, 9870 (1996).
- ²⁵ J. A. Borchers, J. A. Dura, J. Unguris, D. Tulchinsky, M. H. Kelley, C. F. Majkrzak, S. Y. Hsu, R. Loloee, W. P. Pratt, and J. Bass, *Phys. Rev. Lett.* **82**, 2796 (1999).
- ²⁶ Y. Q. Zhan, M. P. de Jong, F. H. Li, V. Dediu, M. Fahlman, and W. R. Salaneck, *Phys. Rev. B* **78**, 045208 (2008).
- ²⁷ I. H. Campbell and B. K. Crone, *Appl. Phys. Lett.* **90**, 242107 (2007).